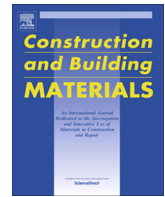




ELSEVIER

Contents lists available at ScienceDirect

Construction and Building Materials

journal homepage: www.elsevier.com/locate/conbuildmat

Sequestration of carbon in pedogenic carbonates and silicates from construction and demolition wastes

Arya Assadi Langrouri^{a,*}, Elizabeth Theron^b, Soheil Ghadr^c^aUniversity of East London, UK^bCentral University of Technology Free State, South Africa^cNational Cheng Kung University, Taiwan

HIGHLIGHTS

- Carbon cycles into Mg/Ca silicates from rubble to form metastable *Ánthropocalc*.
- *Ánthropocalc* microrods are agglomerated 1–4 µm to 15–40 µm nanometric carbonates.
- Calcareous soils with *Ánthropocalc* show high potential for sudden collapse.
- *Ánthropocalc* evolve into more stable polymorphs through carbon sequestration.
- Low collapsibility of soils with calcite slightly rise on carbon sequestration.

ARTICLE INFO

Article history:

Received 13 November 2020

Received in revised form 18 January 2021

Accepted 8 February 2021

Available online 19 March 2021

Keywords:

Sequestration
Anthropogenic
Urban
Calcium carbonate
Soil

ABSTRACT

Progressive diffusion of CO₂ into cement-based construction products and consequent carbon uptake has received considerable attention in recent years. Studies have promoted the capacity of soils mixed with construction cement wastes to function as a carbon sink, which has largely been overshadowed in emissions inventories. There is however little consensus on reversal of carbonation in urban soil systems – that is rooted in uncertainties as to the geo-chemo-mechanical properties of recent carbonates in relation with environmental factors and carbon sequestration. Here, we present preliminary findings from a study of pedogenic and anthropogenic calcium carbonates. In phase 1, we simulate precipitation and weathering of pedogenic and man-made (*Ánthropocalc*) carbonate artefacts. We show that carbon cycles through pedogenic carbonates to reprecipitate snowflake shaped, marginally more soluble, secondary carbonates that occupy the macro-pore spaces. Greater carbon is stored in larger Ca²⁺ sinks. We show that precipitation of carbonates in basic environments containing abundant Na⁺ yields aragonites like carbonates and *Ánthropocalc* artefacts. These are nanometric needle-fibre units that agglomerate into microrods and drape the pore network, lending a high potential of collapsibility. Precipitation of carbonates in acidic environments yield snowflake shaped secondary carbonates of substantially lower collapsibility. These suggest the dominant impacting of pH on shape, form and stability of secondary carbonates, thus opposing the common perception of *Ánthropocalc*'s outright stability. In phase 2, we refer to data compiled from block specimens collected from a demolition site. Long-term exposure to rubble, where sequestration has taken its toll, yields a rise in soil solution pH. Collapsibility increases despite a clear reduction in calcite content and porosity – this is attributed to the meshwork of rodshape elements, dominantly phyllosilicate with needle-shaped *Ánthropocalcs* within the inter-particle space as registered by peaking calcium and oxygen in the EDS data. Data from samples from vegetated sites and in vicinity of rubble highlights a mechanism whereby, *Ánthropocalcs* from carbon sequestration in silicates gradually evolve and change in shape and solubility in response to reduced pH.

© 2021 Elsevier Ltd. All rights reserved.

1. Introduction

The urban built area is globally ubiquitous and expanding. Exploitation of urban grounds has led to changes in soils' engineering properties [26,15,29], and appearance of an array of cations

* Corresponding author at: East Building, Computing and Engineering, Docklands Campus, University of East London, London E16 2RD, UK.

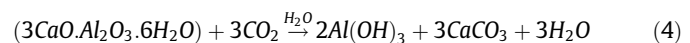
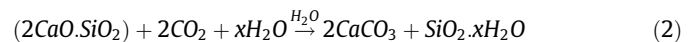
E-mail addresses: A.AssadiLangrouri@uel.ac.uk (A. Assadi Langrouri), etheron@cut.ac.za (E. Theron).

including aluminium, calcium, iron, manganese, magnesium, and phosphorus in form of amorphous and inorganic compounds. Urban soils are proved to be more alkaline, contain relatively higher contents of coarse fragments [23]. The extent of geochemical alterations depends on the type of human interventions and land use [12,24]. Maximum disturbance and changes can be expected to occur in brownfields, and in soils irrigated with urban wastewater. In this, urban soils arguably belong to a new class of soils; the Canadian System of Soil Classification uses the term 'anthroposol' to refer to highly modified soils by human activity [2]. More recently, 'anthropotaltic' soil taxonomy subgroup was proposed for inclusions in soil classification systems in Lo Papa et al. [25].

The distinct geochemical properties of anthroposols have been a stimulus to carbon sequestration and carbonation studies. For example, Assadi-Langroudi [3] compiled and reported a database of CO_3^{2-} level - an indicator for Soil Inorganic Carbon SIC - from 231 soil samples collected from a range of locations at shallow depths. He showed, in comparison with natural soils, urban soils accommodate lower contents of CO_3^{2-} and higher soil solution pH, implying the gradual uptake of carbon dioxide through carbonation by natural minerals as well as cement-based materials abundant in urban soils. Overall, carbonation may lead to formation of four groups of carbonate minerals at the terrestrial biosphere level: first, geogenic carbonates; second, biogenic carbonates (e.g., from terrestrial or aquatic decomposed fauna, flora and microfauna, or in form of Rhizoliths from rhizomicrobial respiration around plant root systems); third, secondary pedogenic carbonates via the Ebelman-Urey unidirectional reaction (Urey 1952, Berner 2004) and upon weathering of Ca and Mg silicates (represented as Ca/MgSiO_3); and forth, pedogenic carbonates (fine re-precipitated carbonates from dissolution of geogenic, biogenic or pedogenic carbonates). The third and fourth types can hardly be differentiated, and are argued to exhibit different hydromechanical properties. They may appear in form of hardly-soluble calcite (in nodule form or encrusted with illuvial clay and palygorskite - [20] or readily-soluble aragonite (in form of thermodynamically metastable rod-shape crystals - [32] polymorphs.

1.1. Sequestration

Pedogenic carbonates in natural form are abundant in shallow soils and appear in form of a top thin 'calcic horizon' [31], particularly near root structures. Carbon dating indicates their long residence times in soils (>30 ka - see [16] and their good stability [36]. Weathering is known to be typically slow; a whole dissolution-reprecipitation cycle typically takes 0.4 to 2 ka [21]. Upon exposure to dissolved bicarbonates from CO_2 in soil, they partially dissolve in soil pore water and then re-precipitate to form secondary Ca^{2+} minerals. Similar dissolution reprecipitation process may take place when Ca-Mg silicates - from rubble wastes - are exposed to dissolved bicarbonates from CO_2 in soil. The only difference between the two processes is the highly basic nature of Ca-Mg silicates (pH varying between 6 and 8 - [29]. Calcium silicate, dicalcium silicate ($2\text{CaO} \cdot \text{SiO}_2$), tricalcium silicate ($3\text{CaO} \cdot \text{SiO}_2$), tricalcium aluminate ($3\text{CaO} \cdot \text{Al}_2\text{O}_3$) and similar hydrated products are abundant in urban soils [37], sizing up to 46.5 Mt a^{-1} in the UK only [10] and partially dissolve and reprecipitate in soil pore water under right conditions. Eq. (1) demonstrates the impacting of excessive carbonation of calcium silicate hydrate and decalcification. Eqs. (2) and (3) demonstrate carbonation of dicalcium silicate and tricalcium silicate (broadly designated as C_2S and C_3S). Eq. (4) shows the carbonation of tricalcium aluminate hydrate.



Sequestration of carbon in Ca/Mg-silicates is common in urban shallow grounds. The product is an intermixture of C_2S , C_3S , C-S-H, $\text{Ca}(\text{OH})_2$ and CaCO_3 of various polymorphs. The calcium carbonate product is in fact human-induced calcrete cements - it contains calcitic coatings and infills and needle-fibre calcites, ranging from 1 to 4 μm (micrite) to 15–40 μm (sparite) and more. Verrecchia and Verrecchia [34] reviewed the genesis and micromorphological signatures of needle-fibre calcites. These resemble Aragonites known for their high solubility in water [4] and are hypothesised here to have a tendency of triggering ground collapsibility. This potential risk is the main emphasis of the present study.

1.2. Anthropocalc: Definition and dilemma

The literature contains scattered references to aragonite-like reprecipitated carbonates from interaction between Ca-Mg silicates and CO_2 in soil. This marks an example of carbon sequestration and formation of secondary carbonates and has recently attracted the attention of geo-environmental workers studying the terrestrial capacities for carbon storage. Recent research into formation and behaviour of these carbonates include Andrews and Schlesinger [1], Kerberg et al. [19] and Ogrinc et al. [30] on the links between soil pH, pCO_2 (i.e. carbon dioxide partial pressure), and dissolved inorganic carbon DIC fluxes; and the work of Moraetis et al. [28] on implications of anthropogenic driven carbon sequestration in soils. However, the insufficient information concerning the long-term stability of Ca^{2+} in re-crystallised secondary carbonates casts some doubts into their carbon storage benefits. The morphological similarities and common basic reprecipitation environment between these secondary carbonates and Aragonites raise a key question: are these modern carbonates soluble and can they, under favouring conditions and extreme cases, trigger an emerging ground collapsibility hazard in the long term?

The emphasis of this paper is on advancing the understanding of possible links between hydromechanical properties of calcium carbonate in soil and their formation environment. In this, the core objective is to reflect, from a micro-to-macro perspective, on the carbon sequestration (25 °C and 1 atm pressure) through studying different polymorphs of calcium carbonate and drawing on engineering implications.

2. Phase 1: Physical modelling

2.1. Materials and methods

In phase 1 of the study, a total of 15 calcareous loamy artificial specimens (ML class in Unified Soil Classification System) were synthesised and tested to determine the impacting of environment on calcium carbonate polymorph type, micromorphological signatures, and their chemical and mechanical behaviour.

Eight specimens contained varied contents of synthesized pedogenic calcium carbonate (i.e., calcite) in primary and secondary reprecipitated forms (series S1 and S2). A further four specimens were synthesised (series S3) to contain aragonite-like calcium carbonate, formed in basic soil solutions with varied pH and sodium to calcium ratio. Specimens contained 65 to 70% quartz silt (ground sand), 10% clay (comprising 8% kaolinite and 2% montmorillonite), and 20 to 25% Na/Ca carbonate. A list of test soil specimens is brought in Table 1. The impacting of Ca^{2+} abundance on stability

Table 1

Phase 1 artificial specimens: physico-chemo-mechanical properties of three main specimen series.

Specimen series S1				Specimen series S2				Specimen series S3			
Silt: Kaolin: Montmorillonite: CaCO ₃				Silt: Kaolin: Montmorillonite: CaCO ₃				Silt: Kaolin: Montmorillonite: Na ₂ CO ₃			
70: 8: 2: 20 (%)				65: 8: 2: 25 (%)				70: 8: 2: 20 (%)			
S1-1	S1-2	S1-3	S1-4	S2-1	S2-2	S2-3	S2-4	S3-1	S3-2	S3-3	S3-4
LL: %	35.98	35.98	35.11	35.11	34.20	34.20	33.65	33.65	51.11	51.11	51.11
PL: %	25.00	25.00	24.88	24.88	24.80	24.80	24.43	24.43	37.97	37.97	37.97
PI: %	10.98	10.98	10.23	10.23	9.40	9.40	9.22	9.22	13.14	13.14	13.14
ρ_d : g.cm ⁻³	1.19	1.11	1.19	1.15	1.13	1.13	1.15	1.16	1.18	1.13	1.20
γ_d : kN.m ⁻³	11.65	10.86	11.67	11.34	11.08	11.08	11.31	13.04	11.65	11.08	11.74
e_0 : -	1.23	1.39	1.23	1.29	1.35	1.34	1.23	1.29	1.23	1.35	1.21
n_0 : -	0.55	0.58	0.55	0.56	0.57	0.57	0.56	0.56	0.55	0.57	0.55
S_r : %	33.62	31.74	33.76	32.07	30.05	32.49	30.05	30.69	33.64	30.05	28.13
¹ pH: -	N/A	N/A	4.7–5.4	4.7–5.3	N/A	N/A	4.7–5.4	4.7–5.2	12.0	12.0	4.0
² pH: -	7.1	7.0	6.8	6.8	7.0	7.1	6.8	6.8	8.0	8.2	6.5
³ pH: -	>7.0	>7.0	<7.0	<7.0	>7.0	>7.0	<7.0	<7.0	>7.0	>7.0	<7.0
V_p : m.s ⁻¹	0.63	0.66	0.65	0.68							
V_s : m.s ⁻¹	0.26	0.27	0.27	0.28							
ρ : kΩ.m	4.36	3.54	2.33	2.30							
⁴ I_{com} : %	0.021		0.088		0.024		0.025		9.35		2.866
⁵ I_{col} : %	N/A	2.154	N/A	2.904	N/A	0.111	N/A	0.396	23.32		0.092
⁶ Ca		60.5		121.0		61.5		64.7	32.4		15.6
⁷ Ca									24,042	24,627	24,240
									24,259	23,266	21,326
									24,206	23,304	23,345
											24,512

LL = Liquid Limit; PL = Plastic Limit; PI = Plasticity Index; ρ_d = dry density; γ_d = dry unit weight; e_0 = initial void ratio; n_0 = initial porosity; S_r = degree of saturation, V_p = compressive wave velocity; V_s = shear wave velocity; ρ = resistivity.

¹pH of reactant solution.

²pH of precipitation environment.

³pH of soil.

⁴Index of compressibility (0–200 kPa).

⁵Index of collapsibility (200 kPa).

⁶in mg.l⁻¹, cation load in outflowed water from specimens after SOT.

⁷in mg.l⁻¹, cation load in CaCl₂ aqueous reactant solution : cycle 1 – cycle 2 – cycle 3.

of carbon stored in secondary carbonates was investigated through three further specimens (series S4), comprising 10% silt and varied contents of kaolinite and calcium hydroxide, compressed and then mediated with carbon dioxide.

2.1.1. The silt fraction

A silt stock which resembled natural periglacial silt in shape, size and grading was prepared in the laboratory by controlled crushing of standard English 400–600 µm Leighton Buzzard sand. Calgon solution (or standard dispersant – that is 33 g Na₂PO₃ blended with 7 g Na₂CO₃ in distilled water forming 1000 ml of solution) was used to remove traces of carbonate from sand. The silt fraction was removed by screening the clean sand through a 63 µm mesh. Oven-dried clean sand was then split into seven batches, each weighing 125 g, and crushed in a high-energy disc mill (also known as vibrating cup mill) for a total grinding duration of 0.5 to 6 min through series of timed grinding-rest-grinding sequences, each lasting 60 s. Disc mill simulates stress conditions similar to that of the glacial abrasion – that is combined abrasion between sand particles' sharp edges, and also among particles and rotating smooth tungsten carbide pestle – see Assadi-Langroudi et al. [6].

Particle and mode size distribution were derived at the end of each grinding experiment, using a combination of Laser Diffraction (LD) spectroscopy (for grains sizing 2.5 to 50 µm), Sedigraph (for > 50 µm particles), and pipette (for sub-2.5 µm particles) methods – see Stott and Theron [33]. Laser Diffraction (LD) granulometry (or Low Angle Laser Light Scattering LALLS) was performed on crushed sand samples using a Malvern Mastersizer 2000 with Hydro MU and ultrasonic attachment at Durham University. A Micromeritics Sedigraph 5000ET at Newcastle University was used to study the grading of > 50 µm particles. Pipette tests were

conducted at Newcastle University. Fig. 1 illustrates the particle and mode size distribution of the seven ground crushed sands.

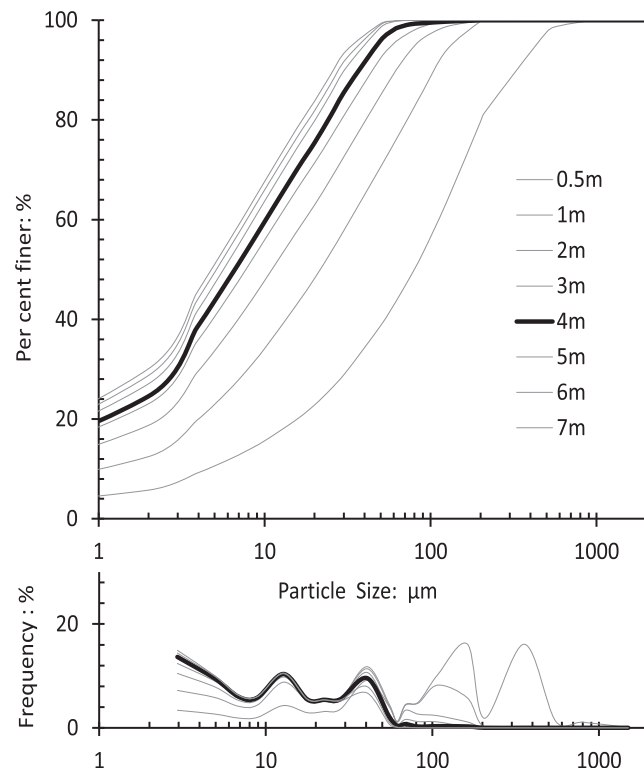


Fig. 1. Particle and mode size distribution of crushed sand material: adopted crushing pattern illustrated in bold line representing 4 min of interrupted grinding.

A total grinding duration of 4 min yielded the maximum 10–20 µm silt populating and hence was adopted as benchmark grinding pattern for production of the silt component of testing specimens. The clay-sized particles were washed out and separated from the crushed sand using sedimentation. The soil–water suspension was vigorously agitated in 1000 ml glass beaker and allowed to stand for predetermined time for the silt-sized fraction to settle; the cloudy water with clay was carefully poured into another beaker with least possible disturbance. The process was repeated several times. The silt fraction was oven-dried, crumbled, and utilized in testing specimens.

2.1.2. Natural and weathered pedogenic calcium carbonate (S1-S2)

Specimen series S1 and S2 contained synthesised pedogenic calcium carbonate combined with 10 wt% clay – that is a combination of 8% kaolinite, 2% Montmorillonite, and 70 wt% of silt.

To this end, sub-2 µm extra-pure laboratory grade CaCO₃ powder was mixed, at 20 wt%, with silt and clay. Gravitational water content was raised to 14.5 ± 0.2% though adding distilled water to the dry mix. Wet mix was kept in sealed bags in desiccator for 24 h to mellow, before its placement into 75 mm-dia oedometer ring via spooning and static compression. A standard energy of 618 kN·m·m⁻³ was applied and retained on specimens for 120 min. Specimens were remoulded at a w/w_{opt} of 0.85 ± 0.05 – that is the ratio of water content to optimum water content –, a high 1.3 ± 0.1 void ratio, a low 11.5 ± 0.2 kN·m⁻³ dry unit weight, and a 0.32 ± 1 placement degree of saturation (see Table 1). The utilised compression effort is equivalent to the 561 N.m (J) standard proctor compaction energy as set in [7,8]. Specimens were then oven-dried for 24 h at 105°. The intention was to partially dissolve and diffuse carbonates throughout the pore network, with reprecipitation occurring around CaCO₃ nucleus (undissolved particles). Similar procedures were followed and reported in Durand et al. [11]. The effectiveness of method was verified here through electron microscopy imaging, presented in subsequent sections.

Fig. 2 shows the particle size distribution of test specimens. To simulate the weathering process, a subset of S1 specimens were mediated by controlled soil gassing, under constant volume conditions. Specimens were inundated in carbonated water at constant volume via alternating rounds of CO₂ – air influx using an in-house built carbon sequestration cell illustrated in Fig. 3. The cell is the modified form of the DCUS cell initially used in Assadi-Langroudi and Yasrobi [5]. The CO₂ was added to distilled water at a constant 12 °C temperature and 0.4 bar pressure to form carbonic acid, dissociate the hydrogen ions and decrease the pH to a low 4.0 – this replicates the interaction between groundwater and carbon dioxide from atmospheric or biotic sources in soil. The pH was retained at 4.0 for 6 h, following which the fluid was removed from the chamber and replaced with distilled water. Specimens were maintained inundated for at least 6 h in distilled water and neutral pH levels. This followed a final course of drying at 85 °C.

To study the impacting of Ca²⁺ cation ionic load on weathering, four further oedometer specimens (S2) were remoulded to similar packing state and following a similar procedure. Specimens contained 25 wt% sub-2 µm CaCO₃, 10 wt% clay (8% kaolinite and 2% Montmorillonite), and 65 wt% quartz silt.

2.1.3. Anthropocalc calcium carbonate (S3)

To differentiate between secondary carbonates from dissolution-reprecipitation of natural pedogenic carbonates and Ca-Mg silicates, this paper proposes the term ‘Anthropocalc’ for the latter type. The term originates from the Greek word *ànthròpos* (man) and the Latin suffix *calc* or *calx* (lime, calcium carbonate). Anthropocalc is a carbonate type in urban grounds and where natural soil is mixed with demolition and construction wastes.

A further two 75-mm diameter oedometer specimens were constructed to similar packing state and following a similar procedure to those of S1 and S2. Specimens comprised 20 wt% sub-2 µm anhydrous sodium carbonate NaCO₃, 10 wt% clay (8% kaolinite and 2% Montmorillonite), and 70 wt% silt. Specimens were compressed to a high 1.2 ± 0.0 void ratio, an 11.6 ± 0.0 kN·m⁻³ dry unit weight, and a 33 ± 3% placement degree of saturation (see Table 1). Statically compressed and oven-dried specimens were inundated via capillary rise and under constant volume conditions, in supersaturated 0.6 M aqueous solution of calcium chloride CaCl₂ (pH = 8.0–9.0, 110.98 g·mol⁻¹ mass) over a course of 9 h, before a 15 h long drying course at 70 °C. This allowed the dissolved Ca²⁺ ions and the CO₃²⁻ to migrate within and between interassemblage pore spaces via capillary rise, and then upwards on evaporation. Chemical treatment was repeated twice (i.e. a total of three wetting–drying cycles) followed by a final round of drying. Specimen series S3 were designed to simulate precipitation of calcium carbonate under strong basic conditions. The calcium chloride solution molar mass and its rest time was designed, on a try and error basis, to simulate carbonation of waste cement (demolished concrete) at a mean 25 °C and slightly higher than atmospheric pressure (i.e., 1.5 bar) CO₂ influx which reportedly leads to a decreased pH of 8 within 24 h depending on cement physicochemical properties [17]. Fig. 2 shows the particle size distribution for specimen series S3.

To study the impacting of pH of the re-precipitation environment, a further two specimens were synthesised (S3-3 and S3-4) to similar packing state, and through lowering the pH of re-precipitation environment to 4.0 by adding dilute hydrochloric acid to the calcium chloride solution during the wetting–drying treatment cycles. To better understand the impacting of Ca²⁺ load on the sequestration process, a further three specimens (S4-1 to S4-3) were prepared through static compression. Silt at 20 wt% was mixed with kaolinite clay at 70 to 50 wt% and 10 to 30 wt% calcium hydroxide (2.24 g·ml⁻¹). The clay and calcium hydroxide were varied at 10 wt% increment. Compressed mixtures were subjected to CO₂ gassing until specimens attained a low pH of 4 to 5. Specimens were then rested in ambient conditions for a period of minimum 14 days for the pH to return to neutral levels, and subjected to chemical mapping.

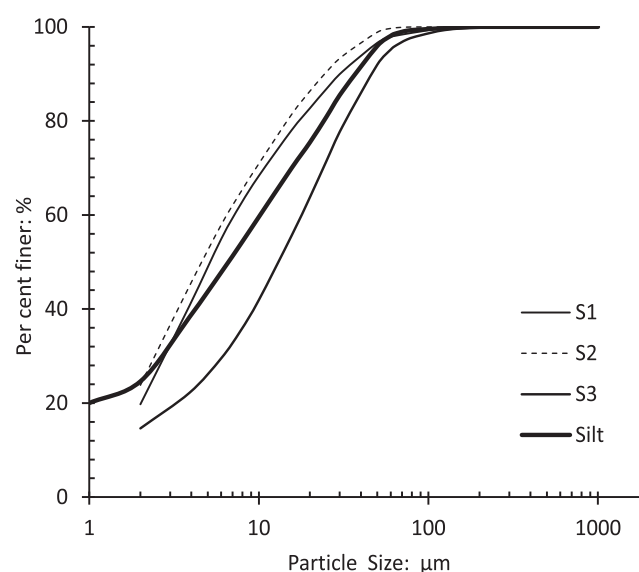


Fig. 2. Particle size distribution curves for three specimen groups (S1-S2-S3) as compared against silt.

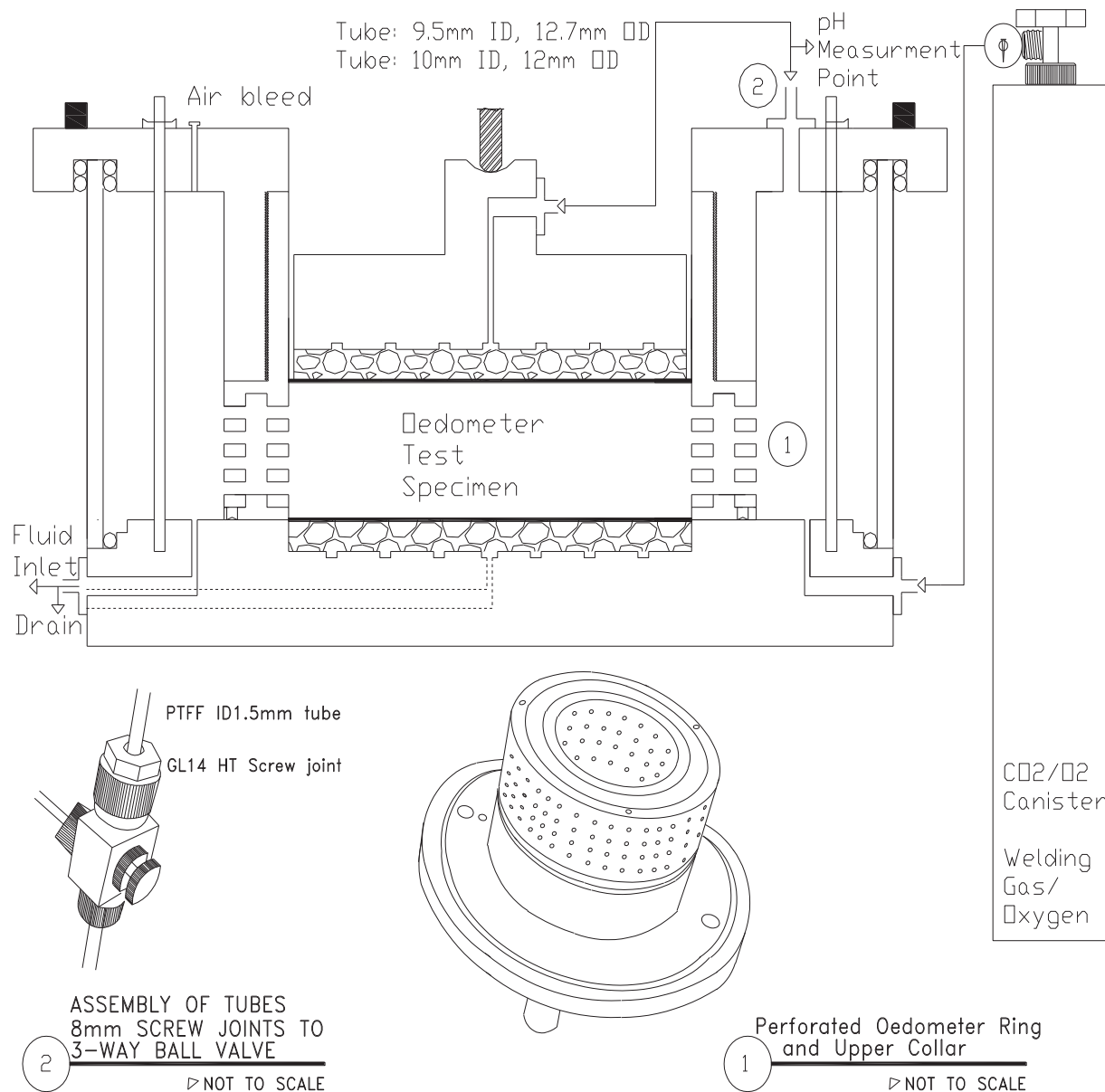


Fig. 3. The in-house carbon sequestration cell used for reconstruction of weathering environment.

2.2. Methods

All specimens were subjected to single oedometer tests (SOT) - standard fashion step-loading (SL). Tests were conducted in compliance with the methodology described in Houston et al. [14]. The SOT data offers an insight into the potential of sudden wetted collapsibility – a problematic soil behaviour that shall be prevented.

To validate the control of Ca²⁺ cation load on polymorph characteristics, an Eijkelkamp calcimeter was used on liquid samples in compliance with the BS 7755-3.9 [9].

Data was paired with microfabric observations made using a Philips XL-30 (LaB6) SEM fitted with an Oxford Instruments INCA EDS system and HKL EBSD system with NordlysS camera. The EDS system was used to establish links between the microfabric of secondary carbonates and chemistry of the precipitation environment.

An insight into the mechanical characteristics of carbonate bonds were established using a portable ultrasonic PUNDIT and

through measuring the velocity of a pulse of ultrasonic longitudinal stress waves (V_p).

Data was paired with electrical resistivity measured in a subset of specimens using the Wenner Array 4-point Method.

For specimen series S3 and to verify the effectiveness of secondary carbonate formation, X-ray diffraction (XRD) analysis was performed on random select bulk samples ($n = 1$, $\lambda = 0.0061$ nm, $V = 40$ kV, 3° to 90° , step 0.015° , count time 0.3 s at 25°C) using a Agilent Technologies SuperNova single crystal X-ray diffractometer with dual wavelength microfocus X-ray sources (Mo and Cu) and an Atlas detector. High-energy short-wavelength radiations were applied to decrease the attenuation. Emphasis was put into detecting minerals with small d-spacing, and as such the low resolution of peak maximal – as a result of using short-wavelengths – was deemed to have negligible effect.

To study the capacity of soil specimens for long-term carbon capture and storage, three sets of Energy Dispersive X-ray Spectrometry (EDS) was performed on three additional soil specimens (S4-1 to S4-3) using an Oxford Energy Dispersive X-ray Spectrometry INCA 700.

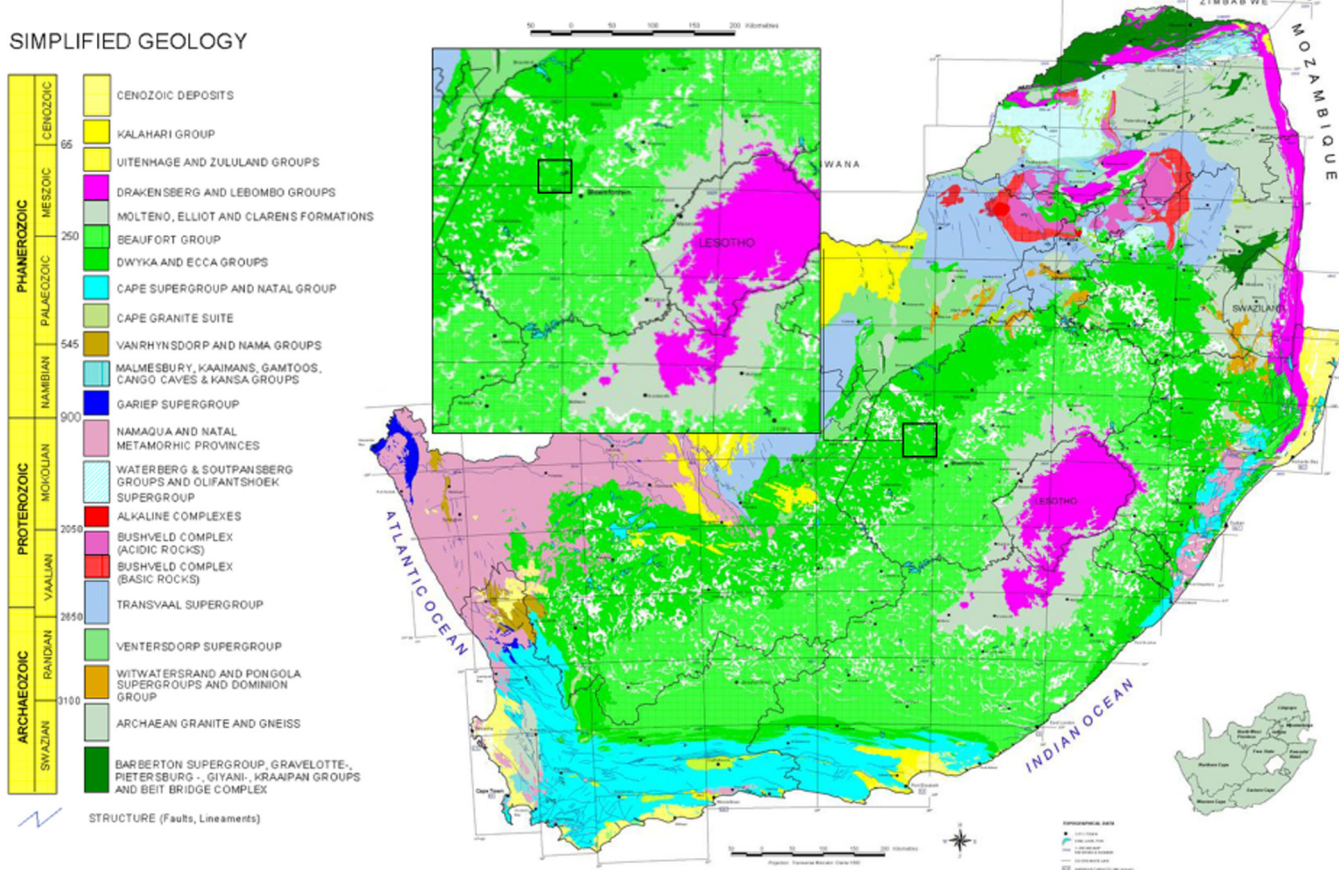


Fig. 4. Location of fieldworks on the simplified geological map of South Africa (compiled by Council for Geoscience – see [36]).

3. Phase 2: Fieldwork

Whilst the physical modelling outcomes offer a valuable insight into the dynamics of calcium carbonate as a function of precipitation environment, the validity of findings remain restricted to artificial soil specimens, thereby inconclusive. To verify the findings, a programme of fieldwork was carried out in north east of Heuwel-sig, is suburb of Bloemfontein, Free States South Africa. The bed-rock across the site is very weathered shale, sandstone, and mudstone with Dolerite intrusions, and belongs to the Adelaide Subgroup of the Beaufort group of the Karroo Super Group. The governing climate is semi-arid, with an annual rainfall of 500 to 550 mm, and temperature ranging from 0 to 29 °C - This is a

favourable environment for shallow residual soils. Fig. 4 illustrates the location of the study site on the 1:250 000 geological map of South Africa. The site was formerly occupied by a concrete building, demolished in 2012 and the rubble has been left mixed with the natural soil for a period of approximately six years. Three trial pits were excavated across the site, each reaching a maximum depth of 1.5 m where most of the carbonation occurs. Trial pits were positioned to allow access to the natural undisturbed soil (zone A), as well as disturbed soil immediately beneath the portlandite rubble (zone B), in vegetated and unvegetated areas. Block samples from depths 30 cm, 60 cm and 90 cm below ground level were collected from each trial pit, sealed, and transported to the laboratory for testing.

Table 2

Phase 2 natural specimens: physico-chemo-mechanical properties of specimens retrieved from block samples.

Depth: mm	TP1				TP2		TP3			
	50	200	300	600	50	300	50	200	300	600
pH	7.0	7.9	7.8	8.0	8.0	7.9	8.5	8.4	8.3	8.4
EC: µ/cm	180	140	190	210	170	120	110	90	80	120
e	0.85	-	0.69	-	0.75	-	-	-	0.38	-
S _f : %	23.2	-	35.9	-	26.5	-	-	-	45.6	-
ρ _d : g/cm ³	1.43	-	1.56	-	1.51	-	-	-	1.92	-
G _s	2.65	-	2.63	-	2.68	-	-	-	2.67	-
w: %	7.5	-	9.42	-	7.5	-	-	-	6.6	-
I _{com} : %	6.91	-	2.28	-	3.71	-	-	-	3.62	-
I _{col} : %	10.89	-	1.24	-	9.99	-	-	-	1.43	-
Quartz	65	-	65	70	39	68	-	-	61	71
Smectite	T	-	2	6	T	T	-	-	T	9
Plagioclase	22	-	19	7	37	21	-	-	23	4
Calcite	T	-	T	3	T	T	-	-	T	8
Clinopyroxene	12	-	8	T	24	11	-	-	15	T

EC = Electrical conductivity; G_s = specific gravity; w = gravitation water content.

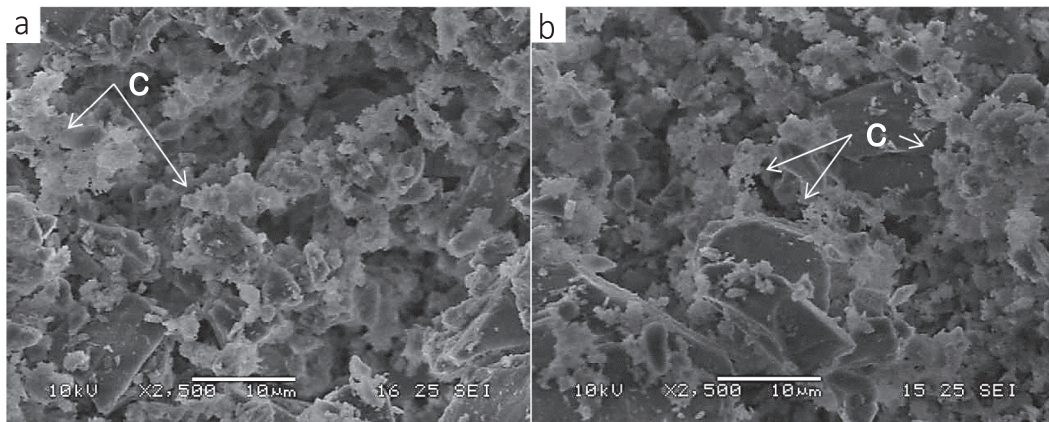


Fig. 5. Snowflake-shaped calcite polymorph in specimen S1, [a] primary calcium carbonates; [b] secondary calcium carbonates in slightly acidic soil solution: 'C' denotes calcite.

Specimens were subjected to SOT to measure their compressibility and collapsibility potential. Geochemical mapping was done through measurement of soil solution pH and EC, mineralogy (XRD, EDS) and microfabric (SEM).

4. Results and discussion

4.1. Physical modelling - pedogenic carbonates

In Table 1, S1-1 and S1-2 represent two identical specimens containing pedogenic carbonates; specimen S1-1 representing the original state and specimen S1-2 representing the post-collapse state of soil specimen. The compressibility and wetted collapsibility (for specimen S1-2) was found to be 7.17% and 2.15% respectively; this represents little collapsibility. The marginal changes to the packing state upon collapse is also reflected in marginal increase in shear wave velocity from 0.255 to 0.269 m.s⁻¹ and the slight decrease in apparent resistivity. Contraction is likely to be associated with collapse of micro-pores, and subsequent increase in coordination number and interlocking as manifested by the marginal increase in the V_s. Events described here lend evidence to the good resistance of pedogenic carbonates to changing stress state and water content.

In Table 1, S1-3 and S1-4 specimens are identical to S1-1 and S1-2; these however were mediated with carbon dioxide to replicate the weathering environment. Collapsibility of weathered specimens was slightly higher at 2.9% point, yet insignificant. On weathering, the apparent resistivity decreased (see specimens S1-1 and S1-3 in Table 1); this can be an indication of contraction at macro-pore's level.

The implications of weathering are visible in SEM micro-graphs at intermediate level (x2500). In Fig. 5a-b, macro-pores appear to be 'stuffed' with snowflake-shaped calcite for original and weathered specimens. In Fig. 5b, dissolved calcites have re-precipitated at particle contact points and formed new inter-particle bridge-shape bonds. The new bonding units probably explains the slightly higher collapsibility seen in carbon dioxide mediated specimens. Although the snowflake shape calcite units remained dominant (Fig. 5b), weathering led to appearance of patchy distributed needle-shaped CaCO₃ units. These aragonite-like polymorphs are known to be more soluble particularly in acidic waters. Liquid limit decreased upon carbonation, indicating a lower water content threshold at which structural collapse occurs on wetting. This is consistent with the modest increase in collapsibility of carbon dioxide mediated specimens (also see Table 1 and Fig. 7)

The weathering is effectively a carbon sequestration process as formulated in Eq. (5).



Theoretically, carbon cycles through calcite units to initially generate calcium hydroxide (Eq. (5)). Carbon further cycles to generate secondary calcium carbonate. If acidic conditions continue to prevail, carbonation results in formation of dilute hydrochloric acid and water, which evaporates into the atmosphere. Fig. 6 shows findings from Energy Dispersive X-ray Spectrometry (EDS). As one would expect, stored carbon increased from 8 to 31% (see specimens S4-1 to S4-3), with increasing calcium cations load from 4 to 10%. This is welcomed in the light of fair stability of primary and secondary calcites as established earlier from the SOT data (see specimen series S1 in Table 1). The gentle decrease in oxygen ionic load from 62 to 50% is probably due to formation of water molecules on interaction of liberated oxygen from calcium hydroxide tails with free -OH anions, which then evaporates into the atmosphere. The remainder oxygen ions interact with carbon dioxide to form dilute hydrochloric acid that balances the pH to neutral levels, ahead of secondary carbonate precipitation. Given the governing acidic to neutral pH environment, no deprotonation and pozzolanic reaction between clays and carbonates take place.

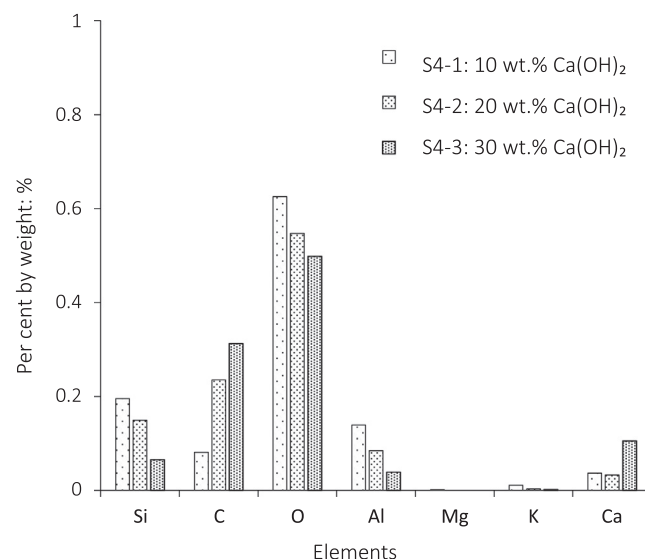


Fig. 6. Atomic concentration of elements in per cent – control specimen series S4 reconstruct the post-gassing precipitation of secondary calcium carbonate.

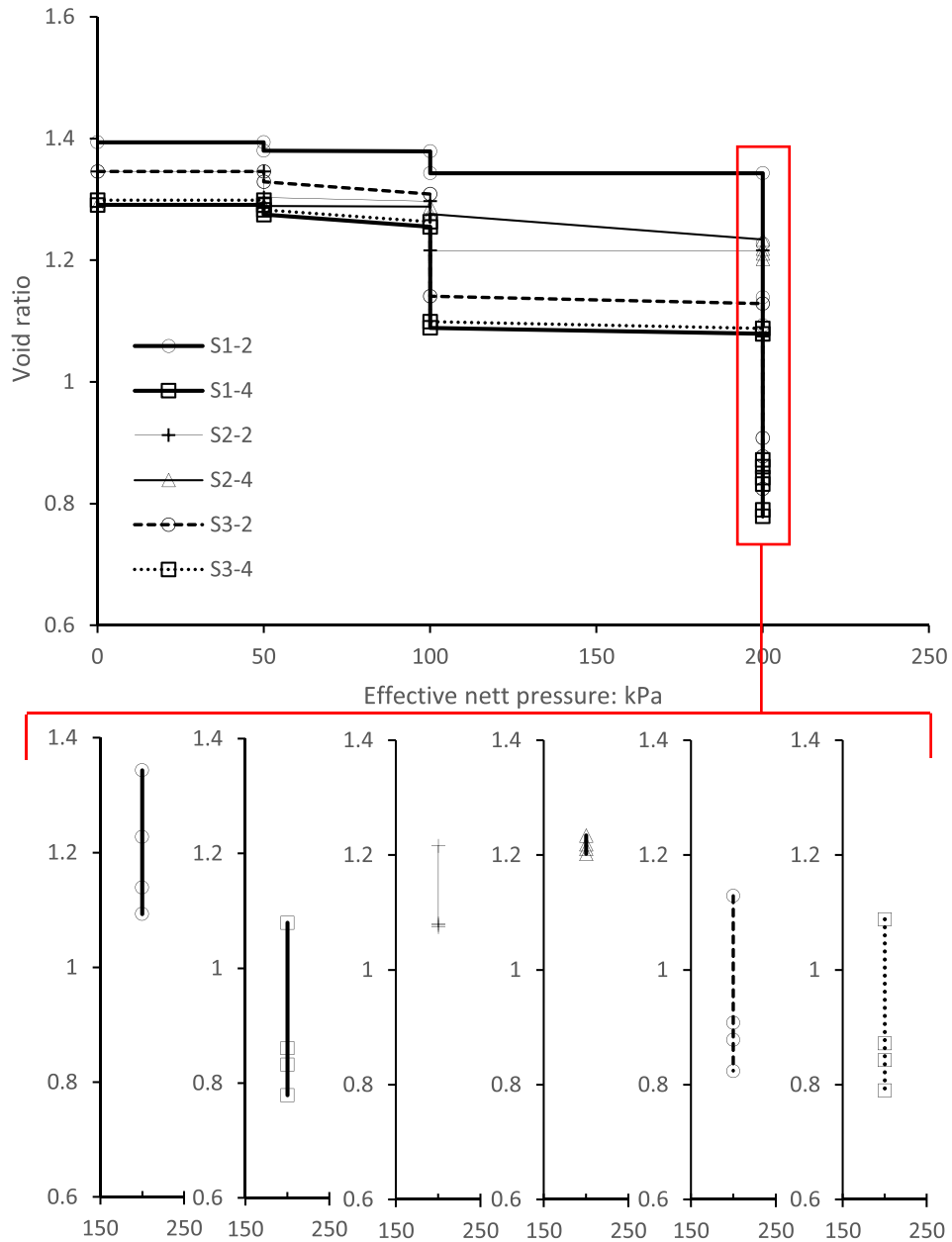


Fig. 7. Variation of void ratio with effective nett stress: Constant water content incremental loading 0–200 kPa followed by wetting at 200 kPa.

4.2. Physical modelling - *Anthropocalc carbonates*

In Fig. 8a-b, needle-shape secondary carbonates are evident in SEM micrograph of S3-1 specimen (series S3); these appear to encrust macro-pores. Fig. 8e shows an explicitly clearer SEM image of needle-shape carbonates in S3-5, which is identical to specimen S3-1 but compacted to much looser state. The looser state and larger macro-voids volume in specimen S3-5 arguably facilitate formation and growth of secondary carbonate crystals. Secondary carbonates here resemble natural aragonites in their iconic needle rod-like shape. Aragonite in soil often appear in form of spheroidal aggregates with radial fibrous structure and rodlike growths of prismatic, pyramidal, and specular crystals [22]. These are typically sub-1 µm thick calcium carbonate units of up to 50 µm length that stabilise the sidewalls of pore channels at shallow depths, but often in deeper calcareous formations too (see Fig. 8c-d for natural aragonites in brickearth samples from South East England). Shorter

and thinner needle-fibre calcite units typically appear in calcareous soils as inter-particle buttress/bridge elements, either encrusting clay-coated quartz sand/silt particles or scaffolding quartz particles for later accumulation of illuviated clay to form reinforced clay bridges.

In the next section, it will be shown that the synthesised secondary carbonates here (Fig. 8a-b) also show micromorphological resemblance with calcium carbonate from weathering of CaOH₂ cement-based demolition wastes (Fig. 8f). Portlandite wastes react with carbon dioxide to form nanometric calcium carbonate needle-fibres, the agglomeration of which eventually forms carbonate microrods draping the soil pore network.

For test specimen S3-1, needle-shape carbonate units were artificially synthesised under slightly basic conditions. Anhydrous sodium carbonate crystallized at particle-to-particle contact points and transformed to calcium carbonate through 3 cycles of wetting-drying with supersaturated calcium chloride solution. The EDS

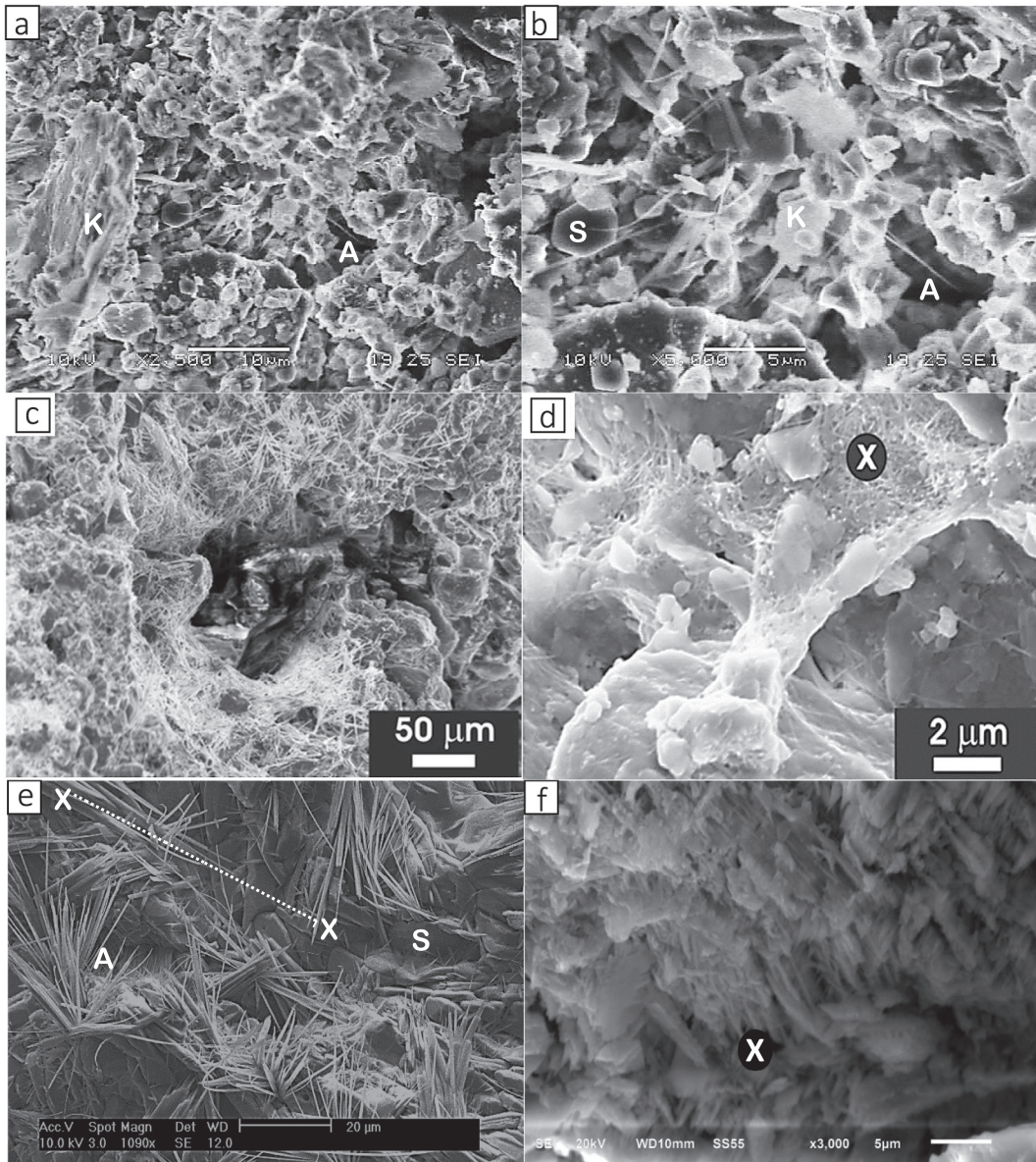


Fig. 8. Primary and secondary calcium carbonates in SEM micrographs: [8a-b] specimen S3-1 - letters A, S and K indicate aragonite/Anthropocalc, silt and kaolinite; [8c-d] meshwork of needle-shaped carbonates lining rootlets and encrusting clay units in shallow non-calcareous deposits south east of England after Milodowski et al., [27]; [8e] artificially synthesised needle-fibre carbonates specimen S3-5, identical to S3-1 but packed to a loose state; [8f] fibrous Anthropocalc from weathered Portlandite wastes in soil sample obtained from Heuwelsig, South Africa.

micrographs (Fig. 9) show the intensity of four key elements along the X-X section line in SEM image in Fig. 8e. At any of the four mark points (3, 23, 33, and 61 μm from origin) on the X-X section line, the intensity of the reemitted radiation peaks for C, O²⁻, and Na⁺, confirming the existence of calcium carbonate crystals at the original anhydrous sodium carbonate sites. Re-precipitation takes place under basic conditions stemmed from the CaCl₂ supersaturated solution. X-ray diffraction XRD micrograph in illustrated in Fig. 10. The Bragg equation ($n\lambda = 2d \cdot \sin\theta$) was utilised to determine the d-spacing for a range of diffraction maxima, which were then contrasted with literature. The XRD data confirms the presence of aragonite (marked as 'A') as the dominant calcium carbonate polymorph in specimen series S3. The highest peak in the XRD pattern, on the first sight, appears to indicate the presence of Calcioanhydrite, although it can more likely be another diagnostic peak of aragonite [32] or quartz (already identified), the sum of both, or Tobermorite as a valid analogy for C-S-H of low Ca/Si ratio [18].

The aragonite phase does not exhibit crystalline behaviour as the associated diffraction peaks are wide with low intensity, typical of low crystalline or amorphous phases.

From the standard SOT test, specimen S3-2 showed a substantially higher 23% wetted collapsibility (Fig. 7), highlighting the good resistance of carbonate units to loading under dry conditions and their rapid dissolution in water. On mediation with carbon dioxide, carbonates dissolve and reprecipitate to form a much more stable form of secondary carbonates (specimen S3-3). Fig. 11 shows that carbon dioxide mediated specimens still contain traces of needle-shaped carbonates, but the dominant shape appears to be snowflake and nodular – similar to that seen for specimen series S1. In fact, in carbon dioxide mediated specimen series S3, collapsibility decreased to lowest levels seen among all other testing calcareous specimens. Following the wetted collapse, the Ca²⁺ load in leachate fluid reduced by almost 50%, indicating a considerable improvement in capacity of soil for carbon storage.

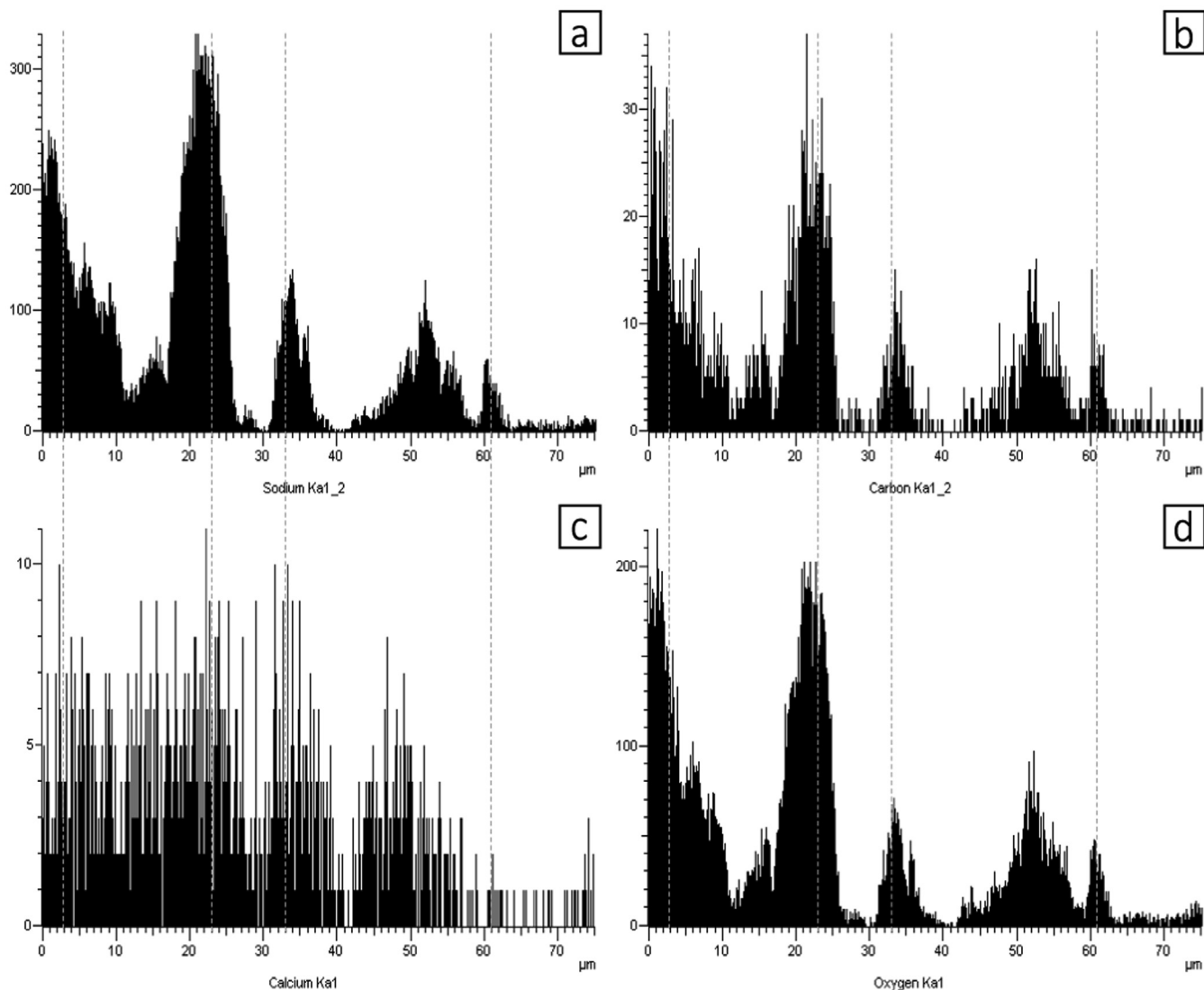


Fig. 9. Synthesised Anthropicalc: Energy-dispersive X-ray spectroscopy along X-X line cutting into microvoids and tubular carbonate units at 3, 23, 33, and 61 μm marks.

Decreased solubility of carbonates in conjunction with decreased collapsibility shows the significance of pH of precipitation environment in the shape and hydro-mechanical response of secondary calcium carbonates.

4.3. Fieldworks - Anthropicalc carbonates

Soil at TP1 was dark brown clayey silty sand (18% clay, 21% silt, 51% sand and 10% gravel) with lenses of olive-colour residual clay, and represents natural loamy soils similar to specimen S1-1 and S1-2 in the phase 1 of this study. The shrinkage, plastic and liquid limits of particles passed from the 0.425 mm sieve size was 8.3%, 17.7% and 13.5%, yielding an index of plasticity of 31.4%. TP1 was excavated at a 10 m distance from the abandoned and demolished concrete building with construction rubble exposed at surface.

Fig. 12 shows SEM micrograph of specimen retrieved from the 300 mm depth of TP1. In Fig. 12a, the open packing of clean sand and silt particles with clayey fillings are evident. The X-Ray micrograph of silts (site 1 in Fig. 12a) and clays (site 2 on Fig. 12a) are presented in Fig. 12b and 12c, respectively. In Table 2, the soil solution pH, calcite, smectite and quartz content increase with depth in TP1. The relatively greater levels of EC at deeper depths corresponds well with lower contents of plagioclase plg - (Na, Ca)(Si,

Al_3O_8 - and clinopyroxene cpx, higher levels of hydrophilic phyllosilicates and denser state of packing. The high compressibility (represented with I_{com} index) and collapsibility (represented with I_{col} index) at shallow 50 mm depth is partly due to the high porosity and low water content of soil (in the range of 12 to 18% in late winter) and are consistent with values in Table 1 for specimen series S1.

In TP2, the substantially higher levels of plg and cpx is indicative of granite or gabbro aggregates from the crushed concrete and rubble that are mixed with the topsoil. Calcite levels across the profile is trace and the soil solution is relatively more basic than soils at similar depths in the adjacent TP1. The relatively lower compressibility at 50 mm depth is due to soils' enhanced hardness from the plg and cpx minerals. Given the slightly lower void ratio, higher natural degree of saturation and elevated permeability of soil (as contrasted with soil in similar 50 mm depth in the adjacent TP1), one would expect the cementitious bonds to have been washed away through the years. The high 10% coefficient of collapsibility however suggests otherwise.

Fig. 13 shows SEM micrograph of a specimen retrieved from the 300 mm depth of TP2. The specimen is identical to artificial specimens before collapse and prior to CO_2 mediation (S3-1). The SEM micrograph in Fig. 13a shows a densely packed meshwork of

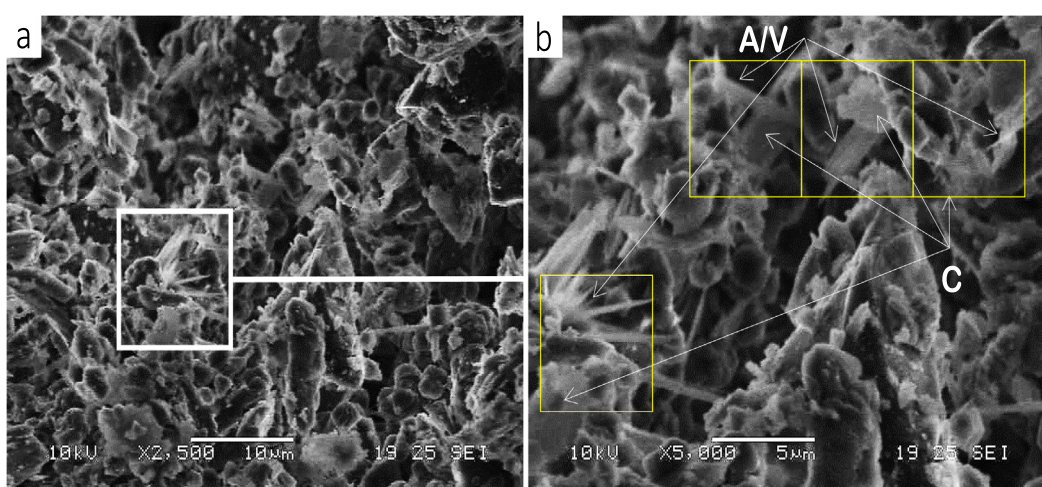
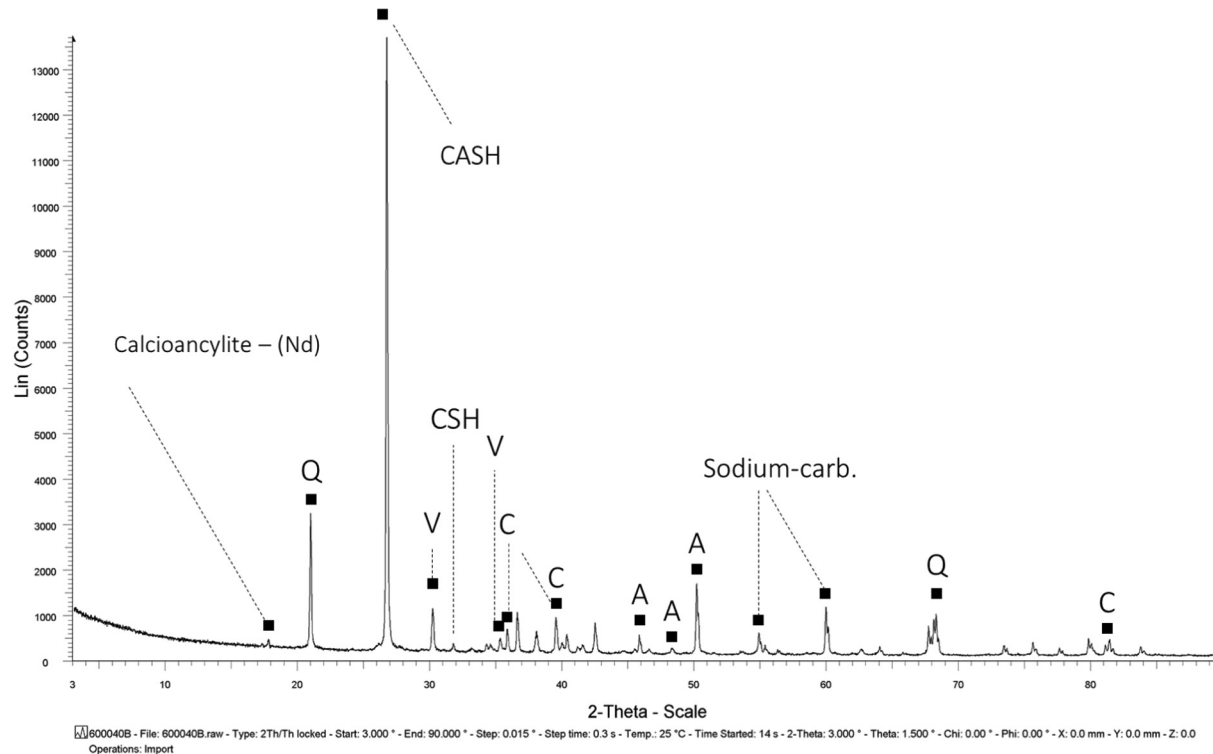


Fig. 11. Synthesised Ánthropocalc: Morphological alteration upon gassing as seen in scanning electron microscopy for specimen S3-3: evolution of needle-shaped A/V into C: A = Aragonite, C = Calcite, V = Vaterite, Q = Quartz.

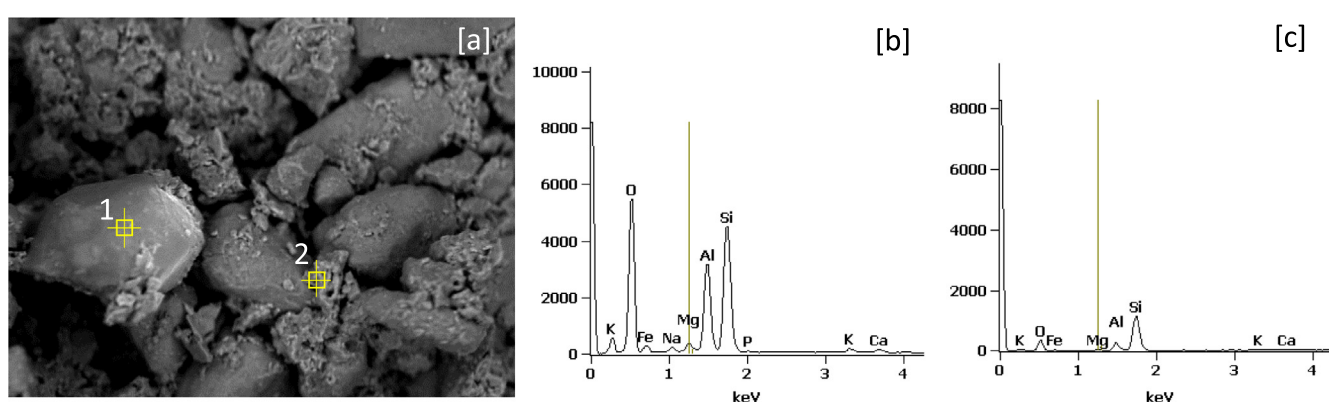


Fig. 12. Microfabric of soil obtained from TP1: [12a] microfabric, silt marked with '1' and clay marked with '2'; [12b] EDX micrograph of silt; [12c] EDX micrograph of clay.

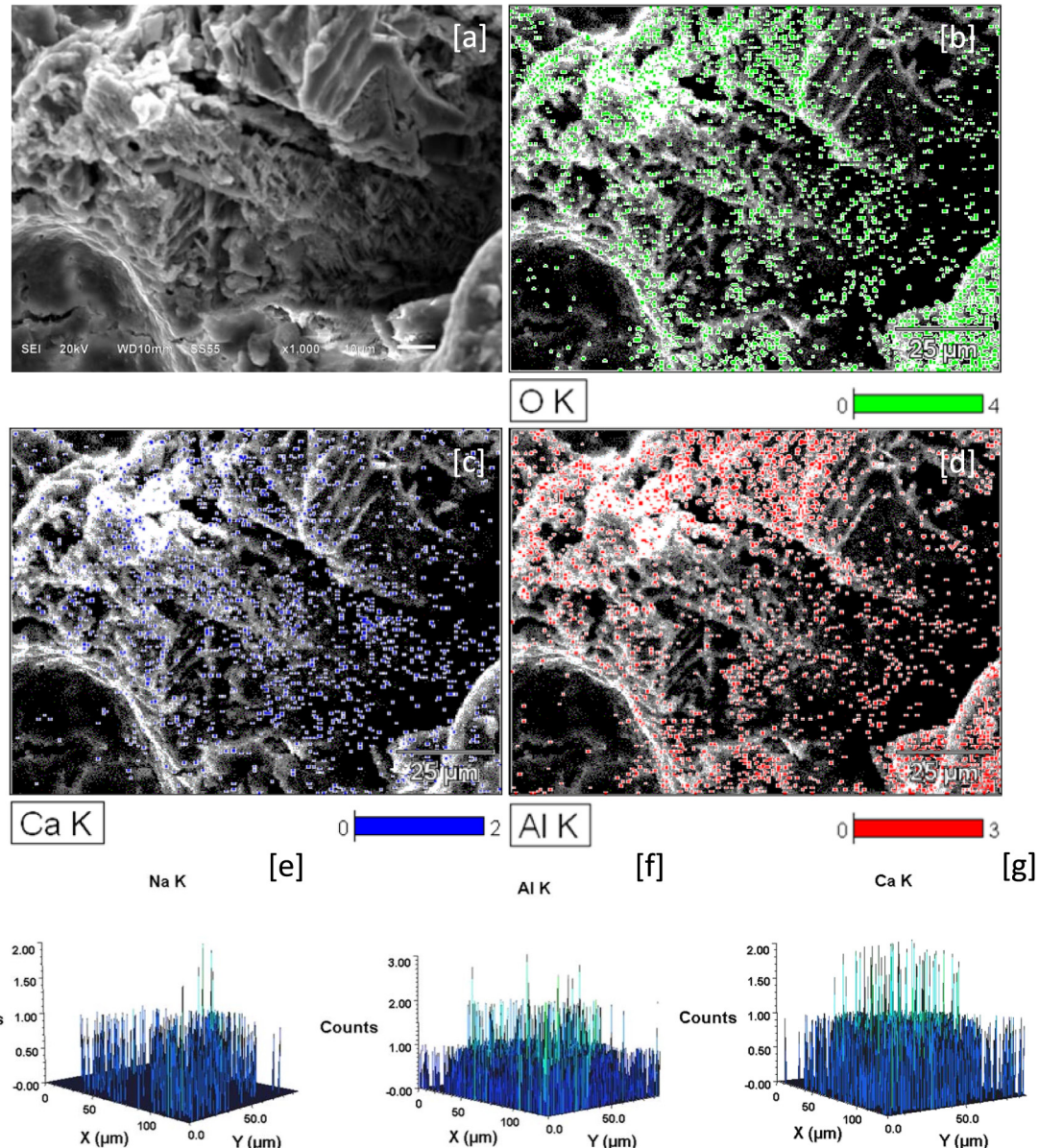


Fig. 13. Microfabric of soil obtained from TP2: [13a] microfabric; [13b-d] projection of ionic distribution on microfabric; [12e-f] spatial distribution of Na, Al, and Ca cations.

rodshape elements of sub-micron thickness that has formed what seems to be a buttress unit between a pair of heavily coated quartz particles. The rodshape elements are similar to those seen in specimen series S3. Contrasting Fig. 13f and 13 g allows distinction between phyllosilicate and calcium carbonate units within the meshwork. Fig. 13b-d illustrate the distribution of aluminium and calcium cations, and the two distinctly peak positions. Fig. 13b-c illustrate the spatial distribution of oxygen and calcium cations on the SEM micrograph and suggests the availability of oxygen cations within the inter-particle space, where calcium cation population peaks. Observations here imply that the meshwork is predominantly of phyllosilicate type but also contains traces of needle-shaped calcium carbonate polymorphs similar to those seen in Fig. 8a-b. TP2 was excavated immediately adjacent to the disposed construction rubble and hence the needle-shaped carbonates – that did not exist in similar depths at TP1 – should be deemed a product of cement-based demolition wastes, thereby can be classified as Ánthropócalc. Similar observations were recently reported in Frankeová and Koudelková [13]. It is worth

to take note of the correlation between high collapsibility and Ánthropócalc presence. Both compressibility and collapsibility decrease in TP3 at the 300 mm depth. Soil here is similar to TP2 but structurally and chemically altered by vegetation. Soil in TP3 is generally basic with a relatively modest electrical resistivity which is consistent with the impacts of air-filled root channels within shallow depths. Calcite content appears to have increased from trace levels to 8% at 300 mm below ground level. This is indicative of either possible downwards leachate of carbonates as precipitation water penetrates through vertical rootlet channels or the evolution of Ánthropócalc to calcites in more acidic environments.

The slight variation of needle shaped units observed in field and laboratory specimens is probably due to the interference of existing organic matters with physicochemical precipitation. For specimen obtained from TP3, the interference is in form of adsorption of organic molecules within the soil solution by the crystal, inhibiting growth, or in form of development of crystals inside microorganisms, forming a cast of the internal structure.

5. Conclusions

Formation, weathering and stability of *Ánthropócalc* – that is secondary carbonates formed in urban grounds as a result of carbon cycling into Mg/Ca silicates from construction rubble – are studied here experimentally and via a programme of testing on artificial and natural soil samples.

In Phase 1, artificial specimens containing an array of pedogenic and *Ánthropócalc* carbonates are synthesised and tested. Carbon sequestration is replicated using an in-house cell to determine the impacting of environment on carbonate polymorph type, structural signatures, and their evolution. Key findings are summarised below:

- In urban soil, lower levels of CO_3^{2-} and basic conditions imply higher dissolution rates, and greater levels of liberated soil inorganic carbon, SiC .
- Highly basic Ca-Mg silicates partially dissolve and reprecipitate in soil pore water; the process is broadly known as anthropocalcretisation, and yields formation of calcitic coatings and infills, as well as needle-fibre elements, ranging from 1 to 4 μm (micrite) to 15–40 μm , that resemble aragonites in shape and solubility. These are nanometric carbonates with radial fibrous structure, the agglomeration of which forms needle-shape *Ánthropócalc* microrods draping the soil pore network.
- Collapsibility of soils containing *Ánthropócalc* is generally high. When carbon cycles through *Ánthropócalc*, reprecipitation under acidic conditions improves the capacity of soil to store carbon, permanently, reduces collapsibility and evolves the carbonates into more stable calcite form.
- Calcite (i.e., natural pedogenic carbonates) in soil induce little collapsibility upon changing stress state and water content. Upon cycling of carbon through calcite collapsibility increases slightly but remains insignificant. Stored carbon would be higher in presence of Ca^{2+} source.

Declaration of Competing Interest

The authors declare that they have no known competing financial interests or personal relationships that could have appeared to influence the work reported in this paper.

Acknowledgements

This work was partially funded by the European Commission (EU SATURN Action 2 Lot 16b) and partially through the Newton Fund, a joint National Research Foundation, Department of Science and Technology and Royal Society (NRF 170627245562 Grant). Authors thank Dr Mohamed Rouainia, Dr Bunmi Eniola and Dr Christopher Davies for their logistical assistance with the physical modelling conducted at Newcastle University UK, Dr Isabel Arce Garcia for assistance with SEM imaging, and Mr Frank Davies of Durham University for his help with Laser Diffraction Spectrometry analysis. Furthermore, authors would like to thank Dr Frederick Roelofse, Ms Tiani Roelofse, Ms Megan Purchase and Mr Jayson Wingrove for their technical support with microanalytical analysis in South Africa.

References

- [1] J.A. Andrews, W.H. Schlesinger, Soil CO_2 dynamics, acidification, and chemical weathering in a temperate forest with experimental CO_2 enrichment, *Global Biogeochem. Cycles* 15 (1) (2001) 149–162.
- [2] M. Anne Naeth, H.A. Archibald, C.L. Nemirsky, L.A. Leskiw, J. Anthony Brierley, M.D. Bock, A.J. VandenBygaart, D.S. Chanasyk, Proposed classification for human modified soils in Canada: Anthroposolic order, *Can. J. Soil Sci.* 92 (1) (2012) 7–18.
- [3] A. Assadi Langrudi, Micromechanics of collapse in loess PhD Dissertation, University of Birmingham, 2014.
- [4] A. Assadi-Langrudi, I. Jefferson, Collapsibility in calcareous clayey loess: a factor of stress-hydraulic history, *Int. J. Geomat.* 5 (1) (2013) 620–627.
- [5] A. Assadi-Langrudi, S.S. Yasrobi, Drainage Controlled Uniaxial Swelling Cell, ICE Proceedings Geotechnical Engineering 166 (4) (2012) 357–364.
- [6] A. Assadi Langrudi, I. Jefferson, K. O'hara-Dhand, I. Smalley, Micromechanics of quartz sand breakage in a fractal context, *Geomorphology* 211 (2014) 1–10.
- [7] ASTM D698 - 12e2. (2012) Standard Test Methods for Laboratory Compaction Characteristics of Soil Using Standard Effort (12 400 ft-lbf/ft³(600 kN·m/m³)).
- [8] BS EN 13286-2:2010 (2010) Unbound and hydraulically bound mixtures. Test methods for laboratory reference density and water content. Proctor compaction. BSgroup.
- [9] BS 7755-3.9:1995, ISO 11466:1995 (1995). Soil quality. Chemical methods. Extraction of trace elements soluble in aqua regia. BSgroup.
- [10] DCLG, 2007. Survey of arisings and use of alternatives to primary aggregates in England, Demolition and Excavation Waste.
- [11] N. Durand, H.C. Monger, M.G. Canti, (2010). Calcium Carbonate Features, in: Interpretation of Micromorphological Features of Soils and Regoliths. Elsevier, 149–194.
- [12] H. El Khalil, C. Schwartz, O. El Hamiani, J. Kubiniok, J.L. Morel, Boulaarbah, Distribution of major elements and trace metals as indicators of technosolisation of urban and suburban soils, *J. Soils Sediments* 13 (3) (2013) 519–530.
- [13] D. Frankeová, V. Koudelková, Influence of ageing conditions on the mineralogical micro-character of natural hydraulic lime mortars, *Constr. Build. Mater.* 264 (2020) 120205, <https://doi.org/10.1016/j.conbuildmat.2020.120205>.
- [14] S.L. Houston, W.N. Houston, V.E. Zapata, C. Lawrence, Geotechnical engineering practice for collapsible soils, *Geotech. Geol. Eng.* 19 (2001) 333–355.
- [15] J.L. Howard, K.M. Orlicki, Composition, micromorphology and distribution of microartifacts in anthropogenic soils, Detroit, Michigan, *Catena* 138 (2016) 103–116.
- [16] R.M. Kalin, G. Dardis, J. Lowndes, Secondary carbonates in the Antrim basalt: geochemical weathering at 35KyBP, *Geofluids II Conference Extended Abstracts* (1997) 22–25.
- [17] S.K. Kaliyavaradhan, T.C. Ling, Potential of CO_2 sequestration through construction and demolition (C&D) waste - An overview, *Journal of CO₂ Utilization* 20 (2017) 234–242.
- [18] S.K. Kaliyavaradhan, T.-C. Ling, K.H. Mo, CO_2 sequestration of fresh concrete slurry waste: Optimization of CO_2 uptake and feasible use as a potential cement binder, *J. CO₂ Util.* 42 (2020) 101330, <https://doi.org/10.1016/j.jcou.2020.101330>.
- [19] N.J. Karberg, K.S. Pregitzer, J.S. King, A.L. Friend, J.R. Wood, Soil carbon dioxide partial pressure and dissolved inorganic carbonate chemistry under elevated carbon dioxide and ozone, *Oecologia* 142 (2) (2005) 296–306.
- [20] F. Khormali, A. Abtahi, S. Mahmoodi, G. Stoops, Argillic horizon development in calcareous soils of arid and semiarid regions of southern Iran, *Catena* 53 (3) (2003) 273–301.
- [21] Y. Kuzyakov, E. Shevtsova, K. Putovoytov, Carbonate re-crystallization in soil revealed by C-14 labelling: experiment, model and significance for paleo-environmental reconstructions, *Geoderma* 131 (2006) 45–58.
- [22] A.Y. Lein, Authigenic carbonate formation in the ocean, *Lithol. Min. Resour.* 39 (1) (2004) 1–30.
- [23] A. Lehmann, K. Stahr, Nature and significance of anthropogenic urban soils, *J. Soils Sediments* 7 (4) (2007) 247–260.
- [24] M.J. Levin, K.H.J. Kim, J.L. Morel, W. Burghardt, P. Charzynski, R.K. Shaw, Soils within cities, Schweizerbart Science Publishers, IUSS Working Group SUITMA, 2017.
- [25] G. Lo Papa, L.V. Antisari, G. Vianello, C. Dazzi, Soil interpretation in the context of anthropogenic transformations and pedotechniques application, *Catena* 166 (2018) 240–248.
- [26] R. Mazurek, J. Kowalska, M. Gąsiorek, M. Setlak, Micromorphological and physico-chemical analyses of cultural layers in the urban soil of a medieval city - a case study from Krakow, Poland, *Catena* 141 (2016) 73–84.
- [27] A.E. Milodowski, K.J. Northmore, S.J. Kemp, D.C. Entwistle, D.A. Gunn, P.D. Jackson, D.I. Boardman, A. Zoumpakis, C.D.F. Rogers, N. Dixon, I. Jefferson, I.J. Smalley, M. Clarke, The mineralogy and fabric of 'Brickearths' in Kent, UK and their relationship to engineering behaviour, *Bull. Eng. Geol. Environ.* 74 (4) (2015) 1187–1211.
- [28] D. Moraetis, N.V. Paranychianakis, N.P. Nikolaidis, S.A. Banwart, S. Rousseva, M. Kercheva, M. Nenov, T. Shishkov, P. de Ruiter, J. Bloem, W.E.H. Blum, G.J. Lair, P. van Gaans, M. Verheul, Sediment provenance, soil development, and carbon content in fluvial and manmade terraces at Koiliaris River Critical Zone Observatory, *J. Soils Sediments* 15 (2) (2015) 347–364.
- [29] S. Norra, N. Fjer, F. Li, X. Chu, X. Xie, D. Stüben, The influence of different land uses on mineralogical and chemical composition and horzonation of urban soil profiles in Qingdao, China, *J. Soils Sediments* 8 (1) (2008) 4–16.

- [30] N. Ogrinc, T. Kanduč, B. Krajnc, U. Vilhar, P. Simončič, L. Jin, Inorganic and organic carbon dynamics in forested soils developed on contrasting geology in Slovenia—a stable isotope approach, *J. Soils Sediments* 16 (2) (2016) 382–395.
- [31] D.L. Royer, Depth to pedogenic carbonate horizon as a paleoprecipitation indicator, *Geology* 27 (12) (1999) 1123, [https://doi.org/10.1130/0091-7613\(1999\)027<1123:DTPCHA>2.3.CO;2](https://doi.org/10.1130/0091-7613(1999)027<1123:DTPCHA>2.3.CO;2)10.1130/9999.
- [32] M. Singh, S. Vinodh Kumar, S.A. Waghmare, P.D. Sabale, Aragonite–vaterite–calcite: Polymorphs of CaCO₃ in 7th century CE lime plasters of Alampur group of temples, India, *Constr. Build. Mater.* 112 (2016) 386–397.
- [33] P. Stott, E. Theron, Shortcomings in the estimation of clay fraction by hydrometer, *J. South Afr. Inst. Civ. Eng.* 58 (2) (2016) 14–24.
- [34] E.P. Verrecchia, K.E. Verrecchia, Needle-fiber calcite; a critical review and a proposed classification, *J. Sediment. Res.* 64 (3a) (1994) 650–664.
- [35] C.J. Vorster (2003). Simplified geology, South Africa, Lesotho, and Swaziland. Council for Geoscience.
- [36] Y. Watanabe, B.W. Stewart, H. Ohmoto, Organic- and carbonate-rich soil formation 2.6 billion years ago at Schagen, East Transvaal district, South Africa. *Geochim. Cosmochim. Acta* 68 (2004) 2129–2151.
- [37] F. Xi, S.J. Davis, P. Ciaias, D. Crawford-Brown, D. Guan, C. Pade, T. Shi, M. Syddall, J. Lv, L. Ji, L. Bing, J. Wang, W. Wei, K.-H. Yang, B. Lagerblad, I. Galan, C. Andrade, Y. Zhang, Z. Liu, Substantial global carbon uptake by cement carbonation, *Nat. Geosci.* 9 (12) (2016) 880–883.